ACS APPLIED MATERIALS & INTERFACES

Research Article

www.acsami.org

Facile Decoration of Multiwalled Carbon Nanotubes with Hetero-oligophenylene Stabilized-Gold Nanoparticles: Visible Light Photocatalytic Degradation of Rhodamine B Dye

Sharanjeet Kaur, Vandana Bhalla,* and Manoj Kumar*

Department of Chemistry, UGC Sponsored Centre for Advanced Studies-25 1, Guru Nanak Dev University, Amritsar-143005, Punjab, India

Supporting Information

ABSTRACT: A hetero-oligophenylene derivative **3** has been designed and synthesized which forms fluorescent spherical aggregates in mixed aqueous media due to its aggregation-induced emission enhancement characteristics. These fluorescent aggregates act as a ratiometric probe for the detection of gold ions in aqueous media and serve as reactors and stabilizers for the preparation of gold nanoparticles. The *in situ* generated gold nanoparticles have been decorated on multiwalled carbon nanotubes to form AuNPs@MWCNTs nanohybrid materials, which serve as recyclable photocatalysts for carrying out degradation of rhodamine dye in aqueous media.

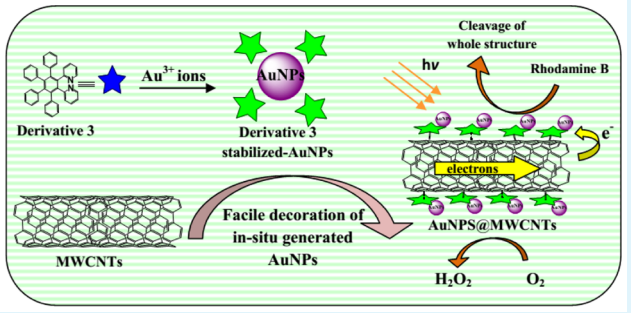

KEYWORDS: *hetero-oligophenylene, aggregation induced emission enhancement, AuNPs, AuNPs@MWCNTs nanohybrid, photocatalysis*

INTRODUCTION

Among various nobel metals, gold occupies a central place in material and supramolecular chemistry due to its applications in catalysis, sensing, nanoelectronics, and surface chemistry.[1−4] Besides, gold complexes and gold nanoparticles (AuNPs), due to their novel chemical properties, have been in use for various biological applications, such as treatment of arthritis and tuberculosis,[5,6] and as carriers for drug and gene delivery systems.[7] However, if accumulated in biological systems at certain concentrations, gold species have potential to disturb various cellular processes.[8−10] Therefore, for studying benign and harmful effects of gold ions, development of suitable methods for their detection is a prerequisite. Among various analytical methods used for detection of gold ions, fluorescence signaling is one of the first choices because of its high sensitivity and selectivity. In this context, various types of fluorescent sensors showing reaction based or coordination based response toward gold ions have been reported in the literature;[11,12,3] however, most of these reported sensors are based on small molecules which show slow response time, low selectivity due to interference from other alkynophilic metals and above all exhibit fluorescence intensity changes relied on single wavelength. Recently, it has been observed that probes based on supramolecular assemblies due to their amplified sensing responses serve as better sensing materials in comparison to those based on small molecules[13−15] and to the best of our knowledge, there is no report in literature showing utilization of supramolecular assemblies as chemosensors for ratiometric detection of gold ions.

Our research work involves development of fluorescent supramolecular assemblies and their utilization for detection of various types of analytes.[16−18] Recently, from our laboratory we reported fluorescent supramolecular assemblies of pentacenequinone derivatives which show "turn-off" response for gold ions and served as reactors for reduction of gold ions to gold nanoparticles (AuNPs).[19,20] The "turn-off" probes generally have interference by fluctuations in background emission resulting in low reliability and sensitivity. Therefore, preparation of "turn-on" fluorescent probes are of vital importance due to their better sensitivity and reliability. Keeping this in mind, we were then interested in the development of fluorescent supramolecular assemblies which could serve as ratiometric "turn-on" sensor for gold ions and for this purpose, we designed and synthesized hetero-oligophenylene derivative **3** having pyridine groups. The hetero-oligophenylene moiety is known to undergo aggregation induced emission enhancement while pyridyl moiety is known for its affinity toward soft metal ions.[21] We envisioned that presence of oligophenylene moiety will impart AIEE characterstics to the molecule and derivative **3** will form supramolecular assemblies in aqueous medium. We further expected that in the presence of soft metal ions the assemblies will become more rigid and could exhibit "turn-on" response toward metal ions. As expected, derivative **3** formed supramolecular aggregates in aqueous media and these

Received: May 14, 2015
Accepted: July 8, 2015
Published: July 9, 2015

DOI: 10.1021/acsami.5b04179
ACS Appl. Mater. Interfaces 2015, 7, 16617−16624

aggregates exhibited ratiometric response toward Au^{3+} ions. During the sensing process these aggregates also served as reactors and stabilizers for the generation of AuNPs. Further, these *in situ* generated AuNPs were decorated on the multiwalled carbon nanotubes to form AuNPs@MWCNTs nanohybrid materials which were then utilized as catalyst for photodegradation of Rhodamine B (RhB) under visible light. Thus, the work being presented here has many advantages, first, unprecedented fluorescent supramolecular assemblies of hetero-oligophenylene derivative **3** have been used as ratiometric "turn-on" sensor for detection of gold ions. Second, the supramolecular assemblies of derivative **3** serve as "not-quenched" reactors and stabilizers for generation of AuNPs. Third, the *in situ* generated AuNPs were used to prepare nanohybrid AuNPs@MWCNTs materials by wet chemical method. Gold nanoparticles supported on carbon nanotubes have received considerable attention due to their potential applications as batteries, supercapacitors, fuel cells, photo voltaic devices, sensors, in photocatalysis, and surface enhanced Raman scattering (SERS).[22−25] Although various methods have been reported for the preparation of AuNPs decorated carbon nanotubes but most of these reported methods suffer from the limitations of requiring longer reaction time, high temperature, use of toxic compounds and multistep reactions. In this context, the method being reported in this manuscript for preparation of AuNPs@MWCNTs nanohybrid materials is convenient and fast over the other reported methods in the literature.[26] Fourth, the present work demonstrates the utility of as prepared AuNPs@MWCNTs nanohybrid materials for degradation of RhB under visible light. The catalytic efficiency of AuNPs@MWCNTs nanohybrid material for photodegradation of RhB was found to be better than the other catalytic systems reported in the literature (Table S3, PS-19 Supporting Information).

RESULTS AND DISCUSSION

Target compound **3** was synthesized via Diels−Alder reaction of 1,2-diphenylethyne (**1**)[27] with 2,5-diphenyl-3,4-di(pyridin-2-yl)cyclopenta-2,4-dienone (**2**)[28] in diphenylether at 240 °C in 71% yield (Scheme 1). The ^{1}H NMR spectrum of compound **3**

Scheme 1. Synthetic Scheme of Hetero-oligophenylene Derivative 3

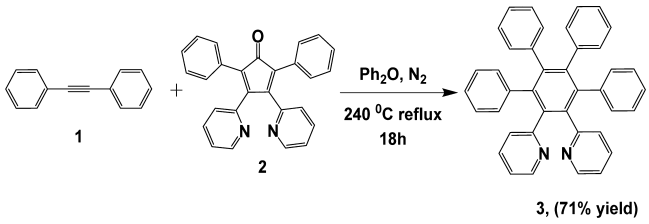

showed two doublets at 8.15 and 6.99 ppm and three multiplets at 7.28−7.20, 6.88−6.82, and 6.75−6.77 ppm corresponding to aromatic protons. A parent ion peak for (M + H^+) was observed at m/z 537.2332 in the ESI mass spectrum. These spectroscopic data corroborate the structure **3** for this compound (Figures S1 to S3 in the Supporting Information).

The UV−vis spectrum of derivative **3** in acetonitrile exhibits absorption bands at 247 and 290 nm due to $\pi-\pi^*$ transitions. However, in the presence of 60% H_2O fraction in CH_3CN, the intensity of the entire absorption spectrum increases gradually and a level-off tail appears in the visible region (Figure 1A).[29] The emission spectrum of derivative **3** in CH_3CN shows a weak emission band at 355 nm (Φ = 0.02). Upon addition of the water fraction up to 60% (volume fraction) to the solution of **3** in CH_3CN, an enhancement in the emission intensity was observed (Φ = 0.21)[30] (Figure 1B). We believe that in aqueous media intramolecular rotations are restricted because of the formation of aggregates which block the nonradiative channels and populate the radiative excitons, thereby making the molecules emissive in their aggregated state. However, the addition of a water fraction higher than 60% leads to a decrease in the emission intensity which may be attributed to the low solubility of derivative **3** in the solvent mixture, thus leading to a decrease in the number of emissive molecules per unit volume.

Further, an increase in fluorescence intensity of compound **3** is observed with increasing fractions of triethylene glycol (TEG) (Supporting Information, Figure S4). This study also supports the AIEE characteristics of derivative **3**. The scanning electron microscopy (SEM) image of derivative **3** in H_2O/CH_3CN (6:4) shows the presence of spherical aggregates (Supporting Information, Figure S5). The dynamic light scattering (DLS) studies indicate the formation of aggregates having average diameter in the range of 500 nm (Supporting Information, Figure S6).

The presence of the pyridyl groups in derivative **3** prompted us to evaluate the binding ability of **3** toward different metal ions, such as Zn^{2+}, Cu^{2+}, Hg^{2+}, Au^{3+}, Fe^{2+}, Fe^{3+}, Co^{2+}, Pb^{2+}, Pd^{2+}, Ni^{2+}, Cd^{2+}, Ba^{2+}, Mg^{2+}, Ag^{+}, Al^{3+}, Ca^{2+}, K^{+}, and Na^{+}, as both their perchlorate and chloride salts using UV−vis and fluorescence spectroscopy. Upon gradual addition of Au^{3+} ions (0−20 equiv) to the solution of **3** (5 μM) in H_2O/CH_3CN (6:4, v/v), a new absorption band at 323 nm[31] was observed (Figure 2A) along with a broad absorption band around 550 nm. The absorption band around 550 nm corresponds to the surface plasmon resonance (SPR) band of gold nanoparticles (inset, Figure 2A).[32] The effect of pH on the formation of AuNPs was also investigated by carrying out UV−vis studies of derivative **3** (5 μM) in H_2O/CH_3CN (6:4, v/v) in the presence of Au^{3+} ions at different pH values (pH 3, 7, and 11). It was found that, on increasing the pH from 7 to 11, the SPR around 550 nm appeared quickly; however, no SPR band corresponding to AuNPs appeared at pH 3 (Figure 3A). We believe that at pH 3 protonation of pyridyl nitrogens takes place which restricts the interaction of aggregates of derivative **3** with the Au^{3+} ions.[18] These studies suggest that the formation of AuNPs is more favorable in basic medium. In the fluorescence spectrum, upon addition of 15 equiv of Au^{3+} ions (75 μM) to the solution of **3** (5 μM) in H_2O/CH_3CN (6:4, v/v) mixture, the intensity of the emission band at 355 nm gradually decreased and the intensity of the emission band at 485 nm (Φ = 0.32) increased in a ratiometric manner (Figure 2B and Supporting Information, Figure S7). These spectral changes are accompanied by the color change of the solution from blue to bluish-green (365 nm UV light, inset Figure 2B). Further, by considering the changes in emission intensity at 355 nm (I_{355}) and at 485 nm (I_{485}), a 21-fold fluorescence enhancement was observed at 485 nm. To get insight into the binding interactions between aggregates of derivative **3** and Au^{3+} ions, we carried out ^{1}H NMR studies in $CDCl_3/CD_3OD/D_2O$ (1:6:3). In the ^{1}H NMR spectrum, the pyridyl protons of derivative **3** undergo a downfield shift in the presence of Au^{3+} ions, which proves that Au^{3+} ions interact with aggregates of **3** through the nitrogen atom of the pyridyl rings (Supporting Information, Figure S8 and PS-7). We believe that coordination

DOI: 10.1021/acsami.5b04179
ACS Appl. Mater. Interfaces 2015, 7, 16617−16624

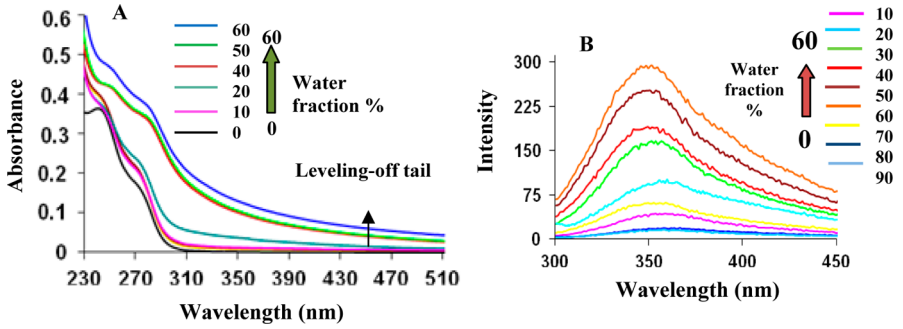

Figure 1. (A) UV−vis spectra of compound **3** (5 μM) showing the variation of absorbance in a H_2O/CH_3CN mixture (0−60% volume fraction of water in CH_3CN. (B) Fluorescence emission spectra of compound **3** (5 μM) in different ratios of H_2O/CH_3CN mixture. λ_{ex} = 290 nm.

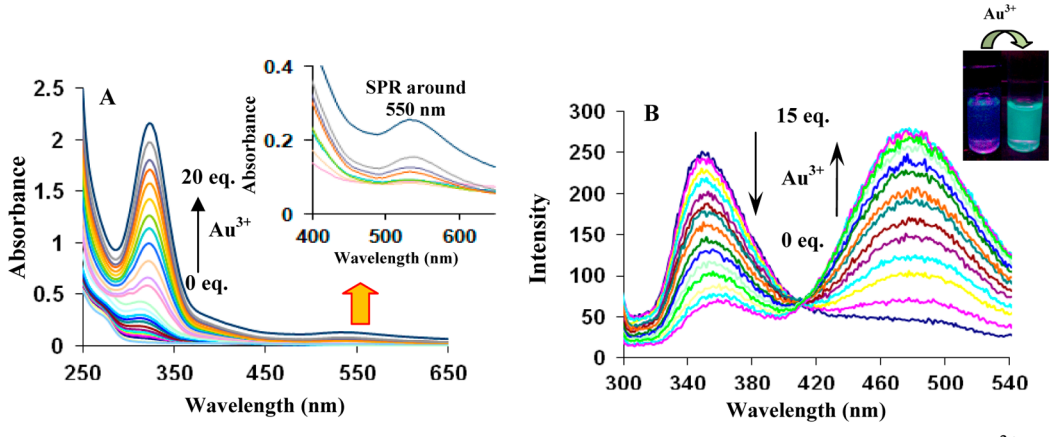

Figure 2. (A) UV−vis spectra of compound **3** (5 μM) upon addition of 20 equiv of Au^{3+} ions in H_2O/CH_3CN (6/4). Inset showing the appearance of a surface plasmon resonance band around 550 nm. (B) Change in the fluorescence spectra of compound **3** (5 μM) upon addition of Au^{3+} in H_2O/CH_3CN (6/4); λ_{ex} = 290 nm. Inset showing the normalized fluorescence intensity (a) before and (b) after the addition of Au^{3+} ions.

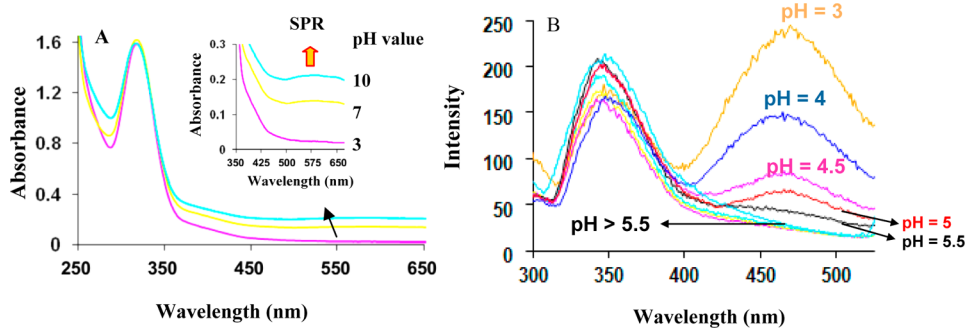

Figure 3. (A) UV−vis spectra of compound **3** (5 μM) after the addition of Au^{3+} ions (0−15 equiv) at different pH values in a H_2O/CH_3CN (6:4, v/v) mixture. (B) Fluorescence emission spectra of derivative **3** (5 μ M) at different pH values in H_2O/CH_3CN (6:4); λ_{ex} = 290 nm.

of Au^{3+} ions with nitrogen atoms of pyridyl groups facilitates the intramolecular charge transfer from electron rich phenyl rings to pyridyl groups, thus leading to fluorescence enhancement at 485 nm.[33] Further, the calibration curve for Au^{3+} showed linearity (R^2 = 0.994) within the concentration range of 0 to 40 μM (Figure S9, Supporting Information). The detection limit of aggregates of derivative **3** for Au^{3+} ions was found to be 36 nM (Supporting Information, Figure S10). This type of ratiometric fluorescence behavior was not observed with the addition of any other metal ions tested, such as Zn^{2+}, Cu^{2+}, Hg^{2+}, Au^{3+}, Fe^{2+}, Fe^{3+}, Co^{2+}, Pb^{2+}, Pd^{2+}, Ni^{2+}, Cd^{2+}, Ba^{2+}, Mg^{2+}, Ag^{+}, Al^{3+}, Ca^{2+}, K^{+}, and Na^{+} as their perchlorate/chloride (Supporting Information, Figure S11). However, in the presence of 15 equiv of Pd^{2+} ions, only the fluorescence quenching at 355 nm was observed (Supporting Information, Figure S11). We also carried out ^{1}H NMR studies of derivative **3** in the presence of Fe^{3+} ions, but no significant change in the spectra was observed (Supporting Information, Figure S12). Thus, aggregates of derivative **3** show high selectivity and high response toward Au^{3+} ions among various other metal ions tested. This high selectivity may be due to much higher standard reduction potential of Au^{3+} ions in aqueous media as compared to that of other metal ions, such as Zn^{2+}, Cu^{2+}, Hg^{2+}, Au^{3+}, Fe^{3+}, Co^{2+}, Pb^{2+}, Pd^{2+}, Ni^{2+}, Cd^{2+}, Ba^{2+}, Mg^{2+}, Ca^{2+}, K^{+}, Na^{+}, etc.[34,35] Fitting the changes in the fluorescence spectra of derivative **3** with Au^{3+} ions using the nonlinear regression analysis program SPECFIT gave a good fit and demonstrated that 1:2 stoichiometry (host/guest) was the most stable species

DOI: 10.1021/acsami.5b04179
ACS Appl. Mater. Interfaces 2015, 7, 16617−16624

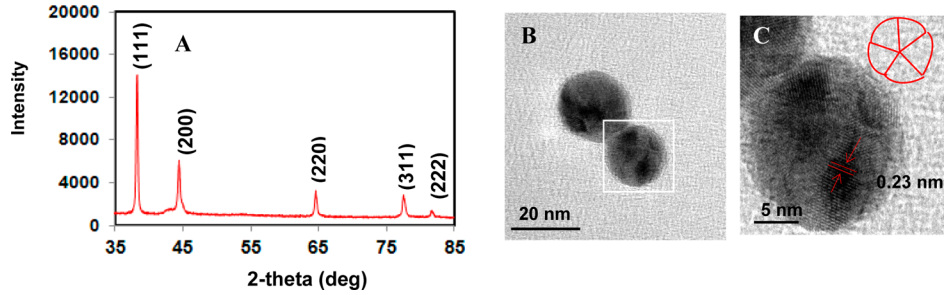

Figure 4. (A) X-ray diffraction pattern of in situ generated AuNPs. (B) Tunneling electron microscopy (TEM) images of in situ generated AuNPs. (C) Magnified view of selected area showing interplanar spacing, reliable with Au fcc, is highlight with red lines. Inset showing the decahedral shape of AuNPs.

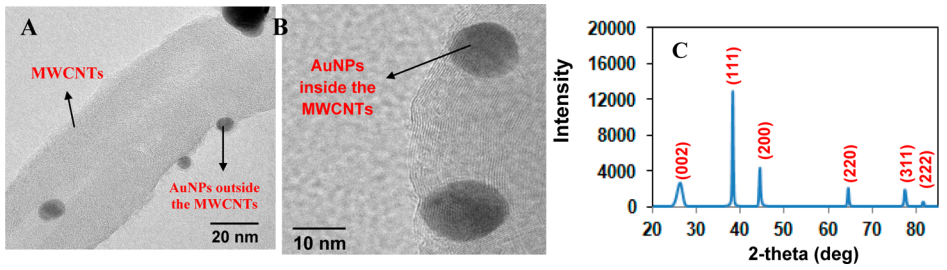

Figure 5. (A and B) TEM and HRTEM images of AuNPs@MWCNTs nanohybrid material, respectively. (C) X-ray diffraction pattern of AuNPs@MWCNT nanohybrid aligned AuNPs on the MWCNTs.

in the solution with the binding constant (log β) = 6.394 ± 0.357.

We also carried out fluorescence studies of derivative **3** at different pH values in a H_2O/CH_3CN (6:4) mixture. It was observed that, at pH below 5.5 (pH 5, 4.5, 4, and 3), a new emission band due to protonation of pyridyl nitrogens appeared at 480 nm.[18] However, no such band appeared at pH > 5.5, which suggests that aggregates of derivative **3** work well in the pH range 5.5 to 12 (Figure 3B). Further, we carried out time-resolved fluorescence studies of derivative **3** in the absence and presence of Au^{3+} ions to determine the radiative (k_f) and nonradiative decay constants (k_{nr}). It was observed that the nonradiative decay constant (k_{nr}) of derivative **3** decreases in the presence of Au^{3+} ions from 0.55×10^9 s^{-1} to 0.11×10^9 s^{-1} (PS-10 and Table S1 PS-17 Supporting Information). These studies clearly show that the presence of gold ions accelerates the decrease in the nonemissive rate constant and the system becomes rigid and more planar in the presence of Au^{3+} ions, which is responsible for emission enhancement at 485 nm.[36]

To get insight into the mechanism of formation of AuNPs, we slowly evaporated the solution of derivative **3** containing AuNPs. After 2 days, a solid dispersion of AuNPs was obtained which was filtered and washed with $CHCl_3$ and THF to remove the organic part. The ^1H NMR spectrum of the organic part of derivative **3** obtained after evaporation of THF and $CHCl_3$ solution shows a downfield shift of aromatic protons (Supporting Information, Figure S14 and PS-11). Based on this ^1H NMR result, we propose that, upon addition of Au^{3+} ions to the solution of aggregates of **3**, Au^{3+} ions interact with nitrogen atoms of pyridyl groups of derivative **3** and get reduced to Au(0). However, no SPR band was observed when UV−vis studies of derivative **3** were carried out in CH_3CN (Supporting Information, Figure S15). Thus, aggregates of **3** function as reducing as well as stabilizing agent for the preparation of nanoparticles at room temperature. To confirm the oxidation of aggregates of derivative **3** in the presence of Au^{3+} ions, we carried out fluorescence studies of aggregates of derivative **3** in the presence of strong oxidizing agent, i.e. *tert*-butyl hydroperoxide; similar ratiometric response was observed as in the case of Au^{3+} ions. This result confirms the oxidation of aggregates of derivative **3** in the presence of Au^{3+} ions (Supporting Information, Figure S16). The powder X-ray diffraction (XRD) analysis of the *in situ* generated gold nanoparticles of derivative **3** (Figure 4A) showed the characterstic pattern of face-centered cubic (fcc) Au(0).[37] The TEM image of the solution of derivative **3** in the presence of Au^{3+} ions showed the presence of decahedral shaped gold nanoparticles (Figure 4B). The DLS data showed the formation of nanoparticles with average diameters in the range of 10−26 nm (Figure S17, Supporting Information).

Having done all this, we were then interested in studying the photocatalytic efficiency of *in situ* generated AuNPs for degradation of organic dyes. RhB was chosen as the representative organic dye due to its low degradability by the conventional methods. Unfortunately, direct use of AuNPs for dye degradation suffers from challenges such as nanoparticle aggregation and post-treatment separation of nanoparticles.[38] Hence, to overcome these problems, we planned to decorate *in situ* generated AuNPs on multiwalled carbon nanotubes (MWCNTs). Due to the good catalytic properties of AuNPs and the excellent electronic properties of MWCNTs, it is expected that the obtained nanohybrids would show enhanced catalytic properties. To prepare AuNPs@MWCNTs nanohybrid, oxidized multiwalled carbon nanotubes and AuNPs solutions were mixed at a 1:1 ratio (3 mL of O-MWCNT (1.5 mg/mL) to 3 mL of 5 mM of AuNPs solution). After 12 h the fine dispersion was obtained. The resulting fine dispersion was expected to contain unbound AuNPs as well. Thus, to remove the unbounded AuNPs present in the supernatant, the disperstion was filtered and washed with a mixture of acetone and ethanol. The complete removal of unbounded AuNPs was

DOI: 10.1021/acsami.5b04179
ACS Appl. Mater. Interfaces 2015, 7, 16617−16624

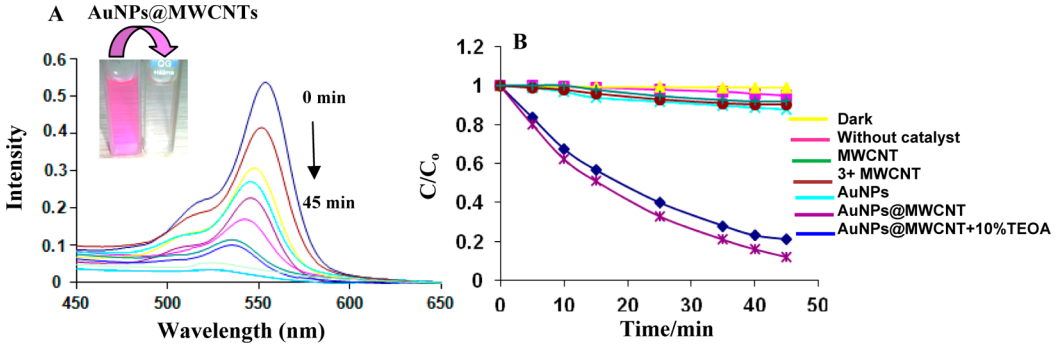

Figure 6. (A) Time-dependent UV−vis absorption spectra for RhB in the presence of AuNPs@MWCNTs nanohybrid under visible-light irradiation and (inset) photographs of the corresponding color change of RhB solutions from red to colorless. (B) The concentration of residual RhB with different visible-light irradiation times in the presence of AuNPs@MWCNTs nanohybrid.

confirmed by recording the UV−vis spectrum of the filterate. It was observed that there was no absorption band corresponding to unbounded AuNPs after first washing (Figure S18, Supporting Information). The adsorption of gold nanoparticles onto the surface of MWCNTs was also confirmed by the UV−vis spectrum of AuNPs@MWCNTs nanohybrid material, which showed disappearance of the surface Plasmon Resonance band (at 550 nm) caused by the plasmon coupling between AuNPs adsorbed on the MWCNTs surface (Figure S19, Supporting Information).[39] The quenched emission of derivative **3** in the fluorescence spectrum of AuNPs@MWCNTs nanohybrid material further confirms the adsorption of AuNPs onto the surface of MWCNTs (Figure S20, Supporting Information).[40,41] Once purified, the AuNPs@MWCNTs nanohybrid materials were resuspended in water and characterized by TEM studies (Figure 5A and B). The HRTEM image of AuNPs@MWCNTs nanohybrid material showed an interplanar spacing of 0.235 nm, which suggests the formation of crystal face-centered cubic (fcc) Au(0) (Figure S21, Supporting Information). The powder XRD pattern also showed the presence of peaks corresponding to the face-centered cubic crystalline gold structure MWCNTs (Figure 5C). The actual loading of gold on MWCNTs in as prepared AuNPs@MWCNTs nanohybrid material was found to be 30.9 wt %, as determined by atomic absorption spectrophotometry (AAS). Further, we believe that the interaction of pyridyl groups of derivative **3** with both the gold and the MWCNTs is responsible for the AuNPs remaining on MWCNTs. This assumption is supported by FT-IR studies which show that the characteristic peaks corresponding to the C═C, C═N, C—C, and C—N stretching modes of pyridyl groups of derivative **3** at 1583, 1438, 1030, and 994 cm^{-1} were shifted to 1601, 1462, 1055, and 1011 cm^{-1}, respectively, for AuNPs@MWCNTs nanohybrid, which indicates that derivative **3** strongly interacts with the MWCNTs, probably through $\pi-\pi$ stacking (Figure S22, Supporting Information).[42]

The photocatalytic activity of AuNPs@MWCNTs nanohybrid was evaluated by the photodegradation of RhB under visible light irradiation after the adsorption−desorption equilibrium between the sample and RhB was achieved. For this the mixture was continuously stirred in the dark for 30 min. For comparison, the blank tests without photocatalyst and without light source were also performed under identical conditions (Figure 6B). It was observed that the degradation of RhB was almost negligible in the absence of catalyst and light source. Further, we compared the performances of AuNPs, MWCNT, and AuNP@MWCNTs hybrid in batch experiments. It was observed that AuNPs and MWCNTs did not show any significant photocatalytic activities (Figure 6B). In contrast photodegradation of RhB was about 98% with the AuNPs@MWCNTs nanohybrid material after 45 min of irradiation. Thus, AuNP@MWCNTs nanohybrid material is responsible for photodegradation of RhB.[43] As shown in Figure 6A, the absorption band of RhB decreased gradually with a slight blue shift ($\Delta\lambda_{max}$ = 15 nm) during photocatalytic degradation, which indicates cleavage of the whole conjugated structure in the degradation process.[44] The degradation of RhB is carried out by hydroxyl radicals which are generated by transfer of electrons and holes from photoactive material to the solution. In the case of electron transfer, generation of hydroxyl radicals requires the presence of oxygen whereas in the case of hole transfer water oxidation is responsible for generation of hydroxyl radicals. To distinguish between the two processes, we added 10% of hole scavenger, i.e. triethanolamine (TEOA),[45,46] to the RhB solution in the presence of the AuNPs@MWCNTs nanocatalysts. Interestingly, no significant change in the degradation of RhB was observed in the presence of TEOA (Figure 6B). This result suggests holes are not the main active species involved in this photochemical degradation process.

The degradation of RhB over AuNPs@MWCNTs was found to be a pseudo-first-order kinetic process (Figure S23, Supporting Information). The reaction rate constant for photocatalytic degradation of aqueous RhB dye by AuNPs@MWCNTs was found to be 0.066 (min^{-1}) (Figure S23, Supporting Information). In comparison, the catalytic photodegradation efficiency of AuNPs@MWCNTs nanohybrid materials was found to be better than that of other reported catalytic systems in the literature (Table S3, PS-19 Supporting Information).

In order to study the photostability of the as-prepared AuNPs@MWCNTs nanohybrid materials, the recycling experiments for the photodegradation of RhB under visible light irradiation were performed. After complete photodegradation of RhB in the presence of AuNPs@MWCNTs nanohybrid, the sample was centrifuged at 4000 rpm for 10 min and filtered through a Millipore filter to recover the catalyst. Interestingly, even after three cycling runs of photodegradation of RhB, no loss in the photocatalytic ability of the AuNPs@MWCNTs nanocomposite was observed (Supporting Information, Figure S24). Further, a TEM image of the nanohybrid catalyst after three runs did not show any significant change in the morphology (Supporting Information, Figure S25). These results demonstrate that the AuNPs@MWCNTs nanocomposite is stable during the photocatalytic process.

DOI: 10.1021/acsami.5b04179
ACS Appl. Mater. Interfaces 2015, 7, 16617−16624

CONCLUSIONS

We designed and synthesized AIEE active hetero-oligophenylene derivative **3**, which formed fluorescent aggregates in aqueous media. Interestingly, these aggregates served as an excellent ratiometric probe for the detection of gold ions among various metal ions tested. Further, the aggregates of hetero-oligophenylene derivative **3** have been utilized as reactors and stabilizers for the preparation of AuNPs which were then decorated on the multiwalled carbon nanotube to form AuNPs@MWCNTs nanohybrid materials. As prepared AuNPs@MWCNTs nanohybrid materials exhibited excellent catalytic efficiency for photodegradation of RhB under visible light and could be recycled three times without significant loss of catalytic activity in the degradation process.

General Experimental Methods. Materials, Reagentsn and Instrumentation. All reagents were purchased from Aldrich and were used without further purification. UV−vis studies were performed in CH_3CN and distilled water. The UV/vis and fluorescence spectra were recorded with Shimdzu UV-2450 spectrophotometer and Shimadzu RF-5301(PC) spectrofluorophotometer, respectively. The SEM images were recorded from Scanning Electron Microscope (SEM)-Zeiss EV040. The TEM mages was recorded from Transmission Electron Microscope (TEM) - JEOL 2100F. The FT-IR spectra were recorded with VARIAN 660 IR Spectrometer. The dynamic light scattering (DLS) data were recorded with MALVERN Instruments (Nano-ZS). The Time resolved fluorescence spectra were recorded with a HORIBA Time Resolved Fluorescence Spectrometer. Elemental analysis was done using a Flash EA 1112 CHNS/O analyzer from Thermo Electron Corporation. ^1H and ^{13}C NMR was recorded on Bruker AVANCE-II FT NMR-AL 500 MHz spectrophotometer using $CDCl_3$ as solvent and tetramethylsilane $SiMe_4$ as internal standards. Data are reported as follows: chemical shifts in ppm (δ), multiplicity (s = singlet, d = doublet, br s = broad singlet m = multiplet), coupling constants J (Hz), integration, and interpretation. Silica gel 60 (60−120 mesh) was used for column chromatography.

The loading of the gold NPs onto the AuNPs@MWCNTs hybrid materials was measured by atomic absorption spectrophotometer (AAS) (GBC Avanta Ver 1.31). The Sample preparation was performed by reflux-assisted digestion by adding 1 mL of nitric acid to 2 mg of AuNPs@MWCNTs hybrid catalyst to determine the Au content. After treatment with concentrated HNO_3 overnight and heating, the resulting solution was cooled, centrifuged and filtered, and filterate was then diluted by 10 times with deionized water and then aspirated into an air−acetylene flame to measure the possible presence of gold loading. Calibration of the instrument was performed within the linear working range for the analysis of gold with concentration between 5 ppm to 14 ppm. The unknown concentration of the gold in sample was then displayed on the calibration curve.

Fluorescence Quantum Yield. Fluorescence quantum yields were determined using optically matching solutions of diphenylanthracene (Φ_F = 0.9 in cyclohexane) as the standard and the quantum yield was calculated using the equation:

$$\Phi_{Fs} = \Phi_{Fr} \times \frac{1 - 10^{-A_s L_s}}{1 - 10^{-A_r L_r}} \times \frac{N_s^2}{N_r^2} \times \frac{D_s}{D_r}$$

Φ_{Fs} and Φ_{Fr} are the radiative quantum yield of the sample and the reference respectively, A_s and A_r are the absorbance of the sample and the reference respectively, D_s and D_r are the respective areas of emission for the sample and the reference, L_s and L_r are the length of the absorption cell of the sample and the reference respectively and N_s and N_r are the refractive indices of the sample and reference solutions.

Procedure for Analytes Sensing. For each experiment we have taken 3 mL solution which contains solution of derivative **3** in 15 μL of THF diluted with 1185 μL of CH_3CN and 1.8 mL distilled water. UV−vis and fluorescence titrations were performed with 5.0 μM solutions of ligand (15 μL of THF was used for dissolution of the ligand) in H_2O/CH_3CN (6:4, v/v). Typically, aliquots of freshly prepared standard solutions (10^{-1} M to 10^{-3} M) of metal ions such as Au^{3+}, Cu^{2+}, Fe^{2+}, Fe^{3+}, Hg^{2+}, Co^{2+}, Pb^{2+}, Pd^{2+}, Zn^{2+}, Ni^{2+}, Cd^{2+}, Ag^{+}, Ba^{2+}, Mg^{2+}, K^{+}, Na^{+}, and Li^{+} their perchlorate $[M(ClO_4)_x; x = 1-3]$/chloride $[M(Cl)_x; x = 1-3]$ in CH_3CN were added to record the UV−vis and fluorescence spectra.

Fluorescence Lifetime (τ_f) Measurement. The time-resolved fluorescence spectra were recorded with a HORIBA time-resolved fluorescence spectrometer. Decays were monitored at the corresponding emiscsion maximum of the compounds. In-built software allowed the fitting of the decay spectra (χ^2 = 1−1.5) and yielded the fluorescence lifetimes. Decay curves were fitted either as a single exponential or multiexponential functions as

$$F(t) = \sum F_i(0) \exp(-t/\tau_i)$$

where τ_i is the emission lifetime and $F_i(0)$ is the pre-exponential factor of the i^{th} component of the sample.

EXPERIMENTAL DETAILS

Compounds **1**[27] and **2**[28] were synthesized according to a literature procedure.

Synthesis of Compound 3. A solution of 1,2-diphenylethyne **1** (1.4 mmol) and 2,5-diphenyl-3,4-di(pyridin-2-yl) cyclopenta-2,4-dienone **2** (1.4 mmol) in diphenyl oxide (2 mL) was refluxed in an atmosphere of nitrogen. After 18 h, the reaction mixture was cooled to room temperature followed by the slow addition of hexane (5 mL) to the reaction mixture. The hexane was decanted off and the rest of the crude product was purified by column chromatography using $CHCl_3$/hexane (8:2) as eluent to give a beige solid (65%); ^1H NMR (500 MHz, $CDCl_3$): δ = 8.15 [d, J = 5 Hz, 2H, ArH], 7.28−7.20 [m, 2H, ArH], 6.99 [d, J = 10 Hz, 2H, ArH], 6.88−6.82 [m, 20H, ArH], 6.75−6.77 [m, 2H, ArH]; ^{13}C NMR (150 MHz, $CDCl_3$): 120.15, 125.28, 125.39, 126.55, 126.62, 131.09, 131.22, 134.29, 139.37, 139.87, 140.04, 141.19, 147.69, 159.07; ESI-MS: Calculated: 536.2252; Found: 537.2332 $(M+1)^+$; Elemental analysis: Calcd for $C_{40}H_{28}N_2$: C 89.52; H 5.26; N 5.22; Found: C 89.31%; H 5.01%, N 5.11.

Synthesis of Gold Nanoparticles. To a 3 mL solution of derivative **3** (0.2 mM) was added 720 μL of 10^{-2} M solution of Au^{3+} ions in H_2O/CH_3CN (6:4, v/v) mixture. The reaction was allowed to stir at room temperature until the color of the solution changes from yellow to purple visible to naked eye.

Synthesis of MWNT/Au Nanohybrid. The MWCNTs (100 mg) were pretreated by sonication in 10 mL of H_2SO_4 (98%) for 2 h. The mixture was then diluted with ice water, the suspension was centrifuged at 4000 rpm for 10 min and the resulting solution was discarded, washed with distilled water until the pH value reached 7, and washed with ethanol. The oxidized-MWCNTs were dried overnight in the oven. Oxidized MWCNTs solution was made by dispersing dried oxidized-MWCNTs in nanopure water and the mixture was sonicated for 30 min until homogeneous dispersion was formed. The concentration of O-MWCNTs was 1.5 mg/mL. The homogeneous solution of gold nanoparticle is formed as mention above by using derivative **3** as reducing as well as stabilizing agent in H_2O/CH_3CN (6:4, v/v) mixture. To prepare MWCNT@AuNPs

DOI: 10.1021/acsami.5b04179
ACS Appl. Mater. Interfaces 2015, 7, 16617−16624

nanohybrid, oxidized multiwalled carbon nanotubes and AuNPs solutions were mixed at a 1:1 ratio i.e 3 mL of O-MWCNT (1.5 mg/mL) with 3 mL of 5 mM of AuNPs solution and stirred for 12 h. The product was filtered and washed with acetone and ethanol in order to remove the unbound gold nanoparticles and dried under vacuum to get AuNPs@MWCNTs nanohybrid.

Photocatalytic Measurements. For photocatalytic degradation of Rhodamine B (RhB), the 0.015g of AuNPs@MWCNTs nanohybrid material was added to the beaker containing 50 mL deionized water. After ultrasonication for 30 min, RhB dye (1 mL, 1 mmol/L) was injected to above solution and the mixture was continuously stirred in dark for 30 min, to ensure that a suitable adsorption/desorption equilibrium of the dye on the surface of catalyst had been established. Then, the photocatalytic test was conducted by irradiation with a 300 W tungsten lamp. The samples with different reaction time were taken out and centrifuged and filtered through a Millipore filter to remove the catalyst particles prior to the analysis. The filtrate was analyzed for the absorbance measurements using a Shimadzu UV-2450 PC spectrophotometer.

■ ASSOCIATED CONTENT

Ⓢ Supporting Information

General data, ^{1}H and ^{13}C NMR and mass spectra of derivative **3**, SEM images, UV−visible absorption spectra, PL emission spectra, and TEM images. The Supporting Information is available free of charge on the ACS Publications website at DOI: 10.1021/acsami.5b04179.

■ AUTHOR INFORMATION

Corresponding Authors

*(V.B.) E-mail: vanmanan@yahoo.co.in.
*(M.K.) E-mail: mksharmaa@yahoo.co.in.

Notes

The authors declare no competing financial interest.

■ ACKNOWLEDGMENTS

M.K. and V.B. are thankful to DST (ref no. SR/S1/OC-69/2012) and CSIR (ref no. 02(0083)/12/EMR-II) for financial support. We are thankful to UGC (New Delhi, India) for the "University with Potential for Excellence" (UPE) project. S.K. is thankful to "UGC-BSR" Scheme for providing a fellowship.

■ REFERENCES

(1) Seo, H.; Jun, M. E.; Ranganathan, K.; Lee, K. H.; Kim, K. T.; Lim, W.; Rhee, Y. M.; Ahn, K. H. Ground-State Elevation Approach to Suppress Side Reactions in Gold-Sensing Systems Based on Alkyne Activation. *Org. Lett.* **2014**, *16*, 1374−1377.

(2) Dong, M.; Wang, Y. W.; Peng, Y. Highly Selective Ratiometric Fluorescent Sensing for Hg^{2+} and Au^{3+}, Respectively, in Aqueous Media. *Org. Lett.* **2010**, *12*, 5310−5313.

(3) Do, J. H.; Kim, H. N.; Yoon, J.; Kim, J. S.; Kim, H. J. A Rationally Designed Fluorescence Turn-On Probe for the Gold(III) Ion. *Org. Lett.* **2010**, *12*, 932−935.

(4) Gryparis, C.; Stratakis, M. Gold Nanoparticles-Catalyzed Activation of 1,2-disilanes: Hydrolysis, Silyl Protection of Alcohols and Reduction of Tert-Benzylic Alcohols. *Chem. Commun.* **2012**, *48*, 10751−10753.

(5) Mishulow, A.; Krumwiede, C. A Colorimetric Reaction Between Gold Chloride and Toxins Apparently Indicative of Toxic Strength. *J. Immunol.* **1927**, *14*, 77−80.

(6) Locke, A.; Main, E. R. Investigation of Proposed Colorimetric Method For Titration Of Diphehteria Toxins. JAMA. *J. Am. Med. Assoc.* **1928**, *90*, 259−260.

(7) Kim, C. K.; Ghosh, P.; Rotello, V. M. *Nanoscale* **2009**, *1*, 61−67.

(8) Block, W. D.; Knapp, E. L. Metabolism, Toxicity, And Manner of Action of Gold Compounds in the Treatment of Arthritis: VII. The Effect of Various Gold Compounds on the Oxygen of Rat Tissues. *J. Pharmacol. Exp. Ther.* **1945**, *83*, 275−278.

(9) Lee, M.-T.; Ahmed, T.; Friedman, M. E. Inhibition of Hydrolytig Enzymes by Gold Compounds I. β-Glucuronidase and Acid Phosphatase by Sodium Tetrachloroaurate (III) and Potassium Tetrabromoaurate (III). *J. Enzyme Inhib. Med. Chem.* **1989**, *3*, 23−33.

(10) Jones, J. R. E. A Future Study of the Relation Between Toxicity and Solution Pressure, With Polycelis Nigra as Test Animal. *J. Exp. Biol.* **1940**, *17*, 408−415.

(11) Patil, N. T.; Shinde, V. S.; Thakare, M. S.; Kumar, P. H.; Bangal, P. R.; Barui, A. K.; Patra, C. R. Exploiting the Higher Alkynophilicity of Au-Species: Development of a Highly Selective Fluorescent Probe for Gold Ions. *Chem. Commun.* **2012**, *48*, 11229−11231.

(12) Wang, J. B.; Wu, Q. Q.; Min, Y. Z.; Liu, Y. Z.; Song, Q. H. A Novel Fluorescent Probe for Au(III)/Au(I) Ions Based on an Intramolecular Hydroamination of a Bodipy Derivative and Its Application to Bioimaging. *Chem. Commun.* **2012**, *48*, 744−746.

(13) Maoz, B. M.; Weegen, R. V.; Fan, Z.; Govorov, A. O.; Ellestad, G.; Berova, N.; Meijer, E. W.; Markovich, G. Plasmonic Chiroptical Response of Silver Nanoparticles Interacting with Chiral Supramolecular Assemblies. *J. Am. Chem. Soc.* **2012**, *134*, 17807−17813.

(14) Deka, J.; Mech, R.; Ianeselli, L.; Amenitsch, H.; Cacho-Nerin, F.; Parisse, P.; Casalis, L. Surface Passivation Improves the Synthesis of Highly Stable and Specific DNA-Functionalized Gold Nanoparticles with Variable DNA Density. *ACS Appl. Mater. Interfaces* **2015**, *7*, 7033−7040.

(15) Fujii, S.; Sakurai, K.; Okobira, T.; Ohta, N.; Takahara, A. Synthesis and Characterization of a Calix[4]arene Amphiphilie Bearing Cysteine and Uniform Au Nanoparticle Formation Templated by its Four Cysteine Moieties. *Langmuir* **2013**, *29*, 13666−13675.

(16) Bhalla, V.; Gupta, A.; Kumar, M. Nanoaggregates of a Pentacenequinone Derivative as Reactors for the Preparation of Palladium Nanoparticles. *Chem. Commun.* **2012**, *48*, 11862−11864.

(17) Sharma, K.; Kaur, S.; Bhalla, V.; Kumar, M.; Gupta, A. Pentacenequinone Derivatives for Preparation of Gold Nanoparticles: Facile Synthesis and Catalytic Application. *J. Mater. Chem. A* **2014**, *2*, 8369−8375.

(18) Kaur, S.; Bhalla, V.; Vij, V.; Kumar, M. Fluorescent Aggregates of Hetero-Oligophenylene Derivative as "No Quenching" Probe For Detection of Picric Acid at Femtogram Level. *J. Mater. Chem. C* **2014**, *2*, 3936−3941.

(19) Sharma, K.; Kaur, S.; Bhalla, V.; Kumar, M.; Gupta, A. Pentacenequinone Derivatives for Preparation of Gold Nanoparticles: Facile Synthesis and Catalytic Application. *J. Mater. Chem. A* **2014**, *2*, 8369−8375.

(20) Sharma, K.; Bhalla, V.; Kumar, M. Facile Synthesis of Gold Nanoparticles Using Aggregates of Pentacenequinone Derivative and Their Catalytic Activity for Oxidative Polymerization, Homocoupling and Reduction. *RSC Adv.* **2014**, *4*, 53795−53800.

(21) Mayer, C. R.; Dumas, E.; Miomandre, F.; Renault, R. M.; Warmont, F.; Vigneron, J.; Pansu, R.; Etcheberry, A.; Secheresse, F. Polypyridyl Ruthenium Complexes as Coating Agent for the Formation of Gold and Silver Nanocomposites in Different Media. Preliminary Luminescence and Electrochemical Studies. *New J. Chem.* **2006**, *30*, 1628−1637.

(22) Singh, R.; Premkumar, T.; Shin, J. Y.; Geckeler, K. E. Carbon Nanotube and Gold-Based Materials: A Symbiosis. *Chem. - Eur. J.* **2010**, *16*, 1728−1743.

(23) White, R. J.; Luque, R.; Budarin, V. L.; Clark, J. H.; Macquarrie, D. J. Supported Metal Nanoparticles on Porous Materials. Methods and Applications Chem. *Chem. Soc. Rev.* **2009**, *38*, 481−494.

(24) Karousis, N.; Tagmatarchis, N.; Tasis, D. Current Progress on the Chemical Modification of Carbon Nanotubes. *Chem. Rev.* **2010**, *110*, 5366−5397.

(25) Georgakilas, V.; Gournis, D.; Tzitzios, V.; Pasquato, L.; Guldi, D. M.; Prato, M. Decorating Carbon Nanotubes with Metal or Semiconductor Nanoparticles. *J. Mater. Chem.* **2007**, *17*, 2679−2694.

(26) See Table S2, PS-18 in the Supporting Information.

DOI: 10.1021/acsami.5b04179
ACS Appl. Mater. Interfaces 2015, 7, 16617−16624

(27) Mio, M. J.; Kopel, L. C.; Braun, J. B.; Gadzikwa, T. L.; Hull, K. L.; Brisbois, R. G.; Markworth, C. J.; Grieco, P. A. One-Pot Synthesis of Symmetrical and Unsymmetrical Bisarylethynes by a Modification of the Sonogashira Coupling Reaction. *Org. Lett.* **2002**, *4*, 3199−3202.
(28) Li, Z.; Zhang, L.; Wang, L.; Guo, Y.; Cai, L.; Yu, M.; Wei, L. Highly Sensitive and Selective Fluorescent Sensor for Zn^{2+}/Cu^{2+} and New Approach for Sensing Cu^{2+} by Central Metal Displacement. *Chem. Commun.* **2011**, *47*, 5798−5800.
(29) Tang, B. Z.; Geng, Y.; Lam, J. W. Y.; Li, B.; Jing, X.; Wang, X.; Wang, F.; Pakhomov, A.; Zhang, X. X. Processible Nanostructured Materials with Electrical Conductivity and Magnetic Susceptibility: Preparation and Properties of Maghemite/Polyaniline Nanocomposite Films. *Chem. Mater.* **1999**, *11*, 1581−1589.
(30) Crosby, G. A.; Demas, J. N. The Measurement of Photoluminescence Quantum Yields. *J. Phys. Chem.* **1971**, *75*, 991−1024.
(31) Isaacs, S. R.; Cutler, E. C.; Park, J.-S.; Lee, R. T.; Shon, Y.-S. Synthesis of Tetraoctylammonium-Protected Gold Nanoparticles with Improved Stability. *Langmuir* **2005**, *21*, 5689−5692.
(32) Mafune, F.; Kohno, J.; Takeda, Y.; Kondow, T. Growth of Gold Clusters into Nanoparticles in a Solution Following Laser-Induced Fragmentation. *J. Phys. Chem. B* **2002**, *106*, 8555−8561.
(33) Scheiner, S.; Kar, T. Substituent Effects upon Protonation-Induced Red Shift of Phenyl-Pyridine Copolymers. *J. Phys. Chem. B* **2002**, *106*, 534−539.
(34) Wu, C.-Y.; Horibe, T.; Jacobsen, C. B.; Toste, F. D. Stable Gold(III) Catalysts by Oxidative Addition of a Carbon−Carbon Bond. *Nature* **2015**, *517*, 449−454.
(35) Kundu, A.; Layek, R. K.; Kuila, A.; Nandi, A. K. Highly Fluorescent Graphene Oxide-Poly(vinyl alcohol) Hybrid: An Effective Material for Specific Au^{3+} Ion Sensors. *ACS Appl. Mater. Interfaces* **2012**, *4*, 5576−5582.
(36) Kubota, Y.; Tanaka, S.; Funabiki, K.; Matsui, M. Synthesis and Fluorescence Properties of ThiazoleBoron Complexes Bearing a β-Ketoiminate Ligand. *Org. Lett.* **2012**, *14*, 4682−4685.
(37) Amin, M.; Anwar, F.; Janjua, M. R. S. A.; Iqbal, M. A.; Rashid, U. Green Synthesis of Silver Nanoparticles Through Reduction with *Solanum Xanthocarpum* L. Berry Extract: Characterization, Antimicrobial and Urease Inhibitory Activities Against *Helicobacterpylor*. *Int. J. Mol. Sci.* **2012**, *13*, 9923−9941.
(38) Wang, H.; Dong, Z.; Chongzheng, N. Hierarchical Carbon Nanotube Membrane-Supported Gold Nanoparticles for Rapid Catalytic Reduction of p-Nitrophenol. *ACS Sustainable Chem. Eng.* **2013**, *1*, 746−752.
(39) Hu, C.; Rong, J.; Cui, J.; Yang, Y.; Yang, L.; Wang, Y.; Liu, Y. Fabrication of a Graphene Oxide-Gold Nanorod Hybrid Material by Electrostatic Self-Assembly for Surface-Enhanced Raman Scattering. *Carbon* **2013**, *51*, 255−264.
(40) Subrahmanyam, K. S.; Ghosh, A.; Gomathi, A.; Govindaraj, A.; Rao, C. N. R. Covalent and Noncovalent Functionalization and Solubilization of Graphene. *Nanosci. Nanotechnol. Lett.* **2009**, *1*, 28−31.
(41) Su, Q.; Pang, S.; Alijani, V.; Li, C.; Feng, X.; Mllen, K. Composites of Graphene with Large Aromatic Molecules. *Adv. Mater.* **2009**, *21*, 3191−3195.
(42) Li, Q.; Sun, B.; Kinloch, I. A.; Zhi, D.; Sirringhaus, H.; Windle, A. H. Enhanced Self-Assembly of Pyridine-Capped CdSe Nanocrystals on Individual Single-Walled Carbon Nanotubes. *Chem. Mater.* **2006**, *18*, 164−168.
(43) Li, S.; Yu, X.; Zhang, G.; Ma, Y.; Yao, J.; Keita, B.; Louis, N.; Zhao, H. Green chemical decoration of multiwalled carbon nanotubes with polyoxometalate-encapsulated gold nanoparticles: visible light photocatalytic activities. *J. Mater. Chem.* **2011**, *21*, 2282−2287.
(44) Fan, Y. Z.; Chen, G. P.; Li, D. M.; Luo, Y. H.; Lock, N.; Jensen, A. P.; Mamakhel, A.; Mi, J. L.; Iversen, S. B.; Meng, Q. B.; Iversen, B. B. Highly Selective Deethylation of Rhodamine B on Prepared in Supercritical Fluids. *Int. J. Photoenergy* **2012**, *2012*, 1−7.
(45) Shalom, M.; Inal, S.; Fettkenhauer, C.; Neher, D.; Antonietti, M. Improving Carbon Nitride Photocatalysis by Supramolecular Preorganization of Monomers. *J. Am. Chem. Soc.* **2013**, *135*, 7118−7121.
(46) Liu, S. W.; Yin, K.; Ren, W. S.; Cheng, B.; Yu, J. G. Tandem Photocatalytic Oxidation of Rhodamine B Over Surface Fluorinated Bismuth Vanadate Crystals. *J. Mater. Chem.* **2012**, *22*, 17759−17767.

DOI: 10.1021/acsami.5b04179
ACS Appl. Mater. Interfaces 2015, 7, 16617−16624